


Cite this: *Chem. Sci.*, 2020, **11**, 5323

All publication charges for this article have been paid for by the Royal Society of Chemistry

Biofunctional Janus particles promote phagocytosis of tumor cells by macrophages†

Ya-Ru Zhang,^a Jia-Qi Luo,^b Jia-Xian Li,^a Qiu-Yue Huang,^a Xiao-Xiao Shi,^a Yong-Cong Huang,^b Kam W. Leong,^{bf} Wei-ling He^{*d} and Jin-Zhi Du^{†b}  ^{*ace}

Herein, a versatile strategy for the construction of biofunctional Janus particles (JPs) through the combination of Pickering emulsion and copper-free click chemistry is developed for the study of particle-mediated cell–cell interactions. A variety of biomolecules including bovine serum albumin (BSA), ferritin, transferrin (Tf), and anti-signal regulatory protein alpha antibodies (aSIRP α), etc., can be incorporated into the Janus platform in a spatially defined manner. JPs consisting of Tf and aSIRP α (Tf–SPA1–aSIRP α JPs) demonstrate a significantly improved binding affinity to either macrophages or tumor cells compared to their uniformly modified counterparts. More importantly, Tf–SPA1–aSIRP α JPs mediate more efficient phagocytosis of tumor cells by macrophages as revealed by real-time high-content confocal microscopy. This study demonstrates the potential advantages of JPs in mediating cell–cell interactions and may contribute to the emerging cancer immunotherapy.

Received 26th February 2020
Accepted 4th May 2020

DOI: 10.1039/d0sc01146k

rsc.li/chemical-science

Introduction

The fate and biological performance of synthetic particles are greatly influenced by their nano–bio interfaces.¹ Many studies have shown that particle properties such as the size, shape, surface chemistry, and mechanical stiffness, have profound effects on particle–cell interactions.^{2,3} For example, Chan and co-workers have explored the use of DNA to construct nanostructures with shape-shifting properties so that they can alter folic acid presentation for the optimization of their biological functions.⁴ However, the cell response to nanoparticles is often not determined by single ligand–receptor recognition. In many cases, collective signals of different events initiate the biological

process. For instance, T cell activation requires two simultaneous signals: T cell receptor-specific signals and costimulatory signals.⁵ In this context, different ligands are needed to be incorporated into the design of synthetic particles to obtain desirable particle–cell responses. Schneck's group has pioneered the design and development of synthetic particles as artificial antigen presenting cells (aAPCs) for *in vitro* activation of T cells.^{6,7} As a step forward, Chiang *et al.* incorporated *anti*-CD3, *anti*-CD28 and *anti*-PD-L1 antibodies onto IO@FuDex nanoparticles for simultaneous T-cell activation and checkpoint inhibition for more efficient cancer immunotherapy.⁸ In spite of these advances, the incorporation of different ligands onto the same particle is challenging and may cause unexpected mutual interference to compromise their biological functions.⁹

Janus particles (JPs) that could spatially display ligands of different functions in one single entity may uniquely address this challenge. Developed for various biomedical applications including micro/nanoactuation,^{10–12} biosensing,^{13–15} drug delivery,^{16,17} and theranostics,¹⁸ JPs possess many promising features that are not offered by homogeneous particles. For example, Leong and co-workers developed a gene delivery system based on Janus nanorods that can simultaneously bind plasmid DNA and targeting ligands in separate parts, which avoided potential interference of DNA to the targeting ligands.¹⁹ The same nanorod could bridge the interactions of dendritic cells and T cells.²⁰ The Yu group found that JPs entered cells differently from homogeneous ones, and further unraveled that JPs enabled the activation of T cells more efficiently than particles uniformly coated with the same number of ligands.^{21,22} All the studies demonstrate the potential advantages of JPs in manipulating particle–cell interactions.

^aGuangzhou First People's Hospital, Institutes for Life Sciences, School of Medicine, South China University of Technology, Guangzhou, 510006, China. E-mail: djzhi@scut.edu.cn

^bSchool of Biomedical Sciences and Engineering, Guangzhou International Campus, South China University of Technology, Guangzhou, 510006, China

^cNational Engineering Research Center for Tissue Restoration and Reconstruction, Key Laboratory of Biomedical Materials and Engineering of the Ministry of Education, Key Laboratory of Biomedical Engineering of Guangdong Province, Innovation Center for Tissue Restoration and Reconstruction, South China University of Technology, Guangzhou 510006, China

^dDepartment of Gastrointestinal Surgery, The First Affiliated Hospital, Sun Yat-sen University, Guangzhou, Guangdong, 510080, China. E-mail: hewling@mail.sysu.edu.cn

^eGuangzhou Regenerative Medicine and Health Guangdong Laboratory, Guangzhou 510005, China

^fDepartment of Biomedical Engineering, Columbia University, New York, NY 10027, USA

† Electronic supplementary information (ESI) available. See DOI: 10.1039/d0sc01146k

However, these studies only dealt with the interaction of JPs with a single type of cell.

Many biological processes involve two or more biological entities in nature. For example, APCs such as macrophages are needed to phagocytize tumor cells for efficient antigen presentation.²³ Ligand- and antibody-modified nanoparticles with homogeneous surface presentation have been developed for controlling the interaction of macrophages and tumor cells for effective cancer immunotherapy.^{9,24} However, the study of JP-mediated cell-cell interactions between different types of cells has been largely overlooked. In this study, we demonstrated a versatile strategy for the construction of biofunctional JPs through the combination of Pickering emulsion and copper-free click chemistry (Scheme S1†), and investigated how the JPs affect cell-cell interactions between macrophages and B16F10 tumor cells.

Results and discussion

To construct JPs with copper-free click chemistry, silica particles (SPs) functionalized with azide groups were prepared as reported.²⁵ Three different azide-modified SPs (SPAs) with the sizes of 150 ± 8 nm, 450 ± 10 nm, and 2.30 ± 0.02 μm were obtained (Fig. S1A†), which were denoted as SPA1, SPA2, and SPA3, respectively. Transmission electron microscopy (TEM) showed that the particles have relatively monodisperse size distributions (Fig. 1A and S1C, D†). The immobilization of azide groups was evidenced by the peak at 2100 cm^{-1} in the FTIR spectrum (Fig. 1B), and such a change also slightly increased the particle zeta potential from -42 to -26 mV (Fig. S1B†). Then, the Pickering emulsion method²⁶ using water as the aqueous phase and molten wax as the oil phase was employed

to prepare SPA colloidosomes and precursors of the JPs. Scanning electron microscopy (SEM) images showed that all SPA1, SPA2, and SPA3 formed monolayer distribution on the surface of the colloidosomes (Fig. 1C and S1E, F†).

Subsequent modifications were performed on the as-made colloidosomes to prepare JPs. To confirm the Janus structure, TEM and fluorescence imaging were employed. For TEM observation, Janus nanoparticles (JNPs) made from SPA1 were functionalized with poly(ethylene glycol) (PEG) and ferritin on opposite faces (denoted as PEG-SPA1-ferritin JNPs). As indicated in Fig. 1D, ferritin patches (~ 10 nm) could be seen on one side of PEG-SPA1-ferritin JNPs, which was also confirmed by the enrichment of Fe element in the energy-dispersive X-ray spectroscopy (EDS) mapping mode. For fluorescence imaging, Janus microparticles (JMPs) made from SPA3 were labeled with fluorescein isothiocyanate (FITC) on one hemisphere (denoted as FITC-SPA3 JMPs), and the green fluorescence mainly distributed on one side of the particles (Fig. 1E). We further prepared FITC and rhodamine B (RB)-labeled BSA and attached them to the opposite sides of SPA3 to generate FITC-SPA3-RB JMPs. Fluorescence microscopy observation demonstrated that the green and red fluorescence were mainly distributed in a spatially segregated manner over the surface of the particles, while more even distribution of the two fluorescence was observed in uniform FITC-SPA3-RB UMPs (Fig. S2†). Flow cytometry analysis quantitatively demonstrated that about 84.6% of the particles were simultaneously stained with two different dyes (Fig. 1F). To demonstrate the versatility of the approach, we constructed a series of JPs with different surface properties, as summarized in Table S1.†

Next, JNPs modified with transferrin (Tf) and BSA on opposite sides (denoted as Tf-SPA1-BSA JNPs) were prepared to examine their targeting ability towards B16F10 cells since this cell line overexpresses transferrin receptors (TfRs).²⁷ For fluorescence imaging, FITC-labeled Tf-SPA1-BSA JNPs were used. As shown in Fig. S3,† confocal microscopy demonstrated that FITC-labeled Tf-SPA1-BSA JNPs showed significantly enhanced green fluorescence on the membrane or inside B16F10 cells in comparison with nontargeted FITC-labeled SPA1 particles. However, if the cells were pretreated with free Tf, the cellular uptake of Tf-SPA1-BSA JNPs was obviously reduced due to the competitive binding of free Tf to TfRs. Quantitative analysis with flow cytometry was in good agreement with confocal microscopy imaging (Fig. 2A and B).

Next, we studied the binding affinity of Tf-SPA1-BSA JNPs to B16F10 cells in comparison with their uniformly modified counterparts (denoted as Tf-SPA1-BSA UNPs), in which the same amount of BSA and Tf was attached (Table S3†). Scatchard analysis was used to estimate the dissociation constant (K_D) of Tf-SPA1-BSA JNPs, Tf-SPA1-BSA UNPs, and free Tf.²⁹ As calculated, the K_D values of Tf-SPA1-BSA UNPs and Tf-SPA1-BSA JNPs were 0.70 ± 0.05 nM and 0.20 ± 0.06 nM, respectively, representing approximately 110-fold and 400-fold enhancement in binding affinity in comparison with free Tf ($K_D = 80.38 \pm 1.20$ nM) (Fig. 2C, D and S4†). Such an enhancement demonstrates the multivalent effect of nanoparticle-based systems due to the increased local surface ligand density in nanoparticle-ligand

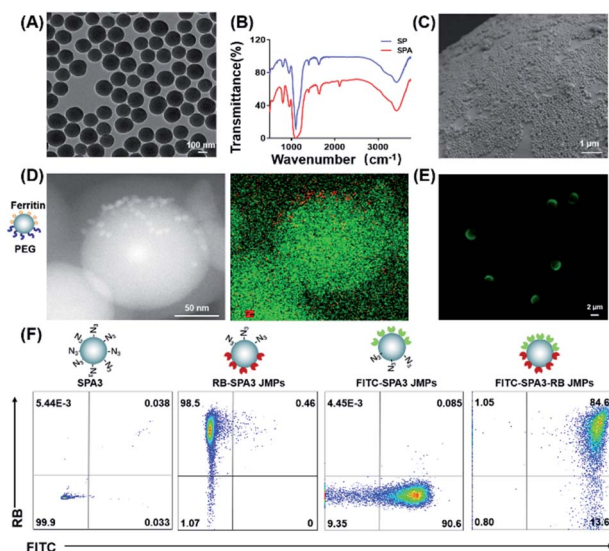


Fig. 1 Preparation and characterization of the biofunctional JPs. (A) TEM image of SPA1. (B) FTIR spectra of SP and SPA. (C) SEM micrograph of a wax colloidosome stabilized by SPA1. (D) Representative TEM images of PEG-SPA1-ferritin JNPs showing the distribution of silicon (green) and iron elements (red). (E) Fluorescence image of FITC-SPA3 JMPs. (F) Flow cytometry analysis of FITC-SPA3-RB JMPs.



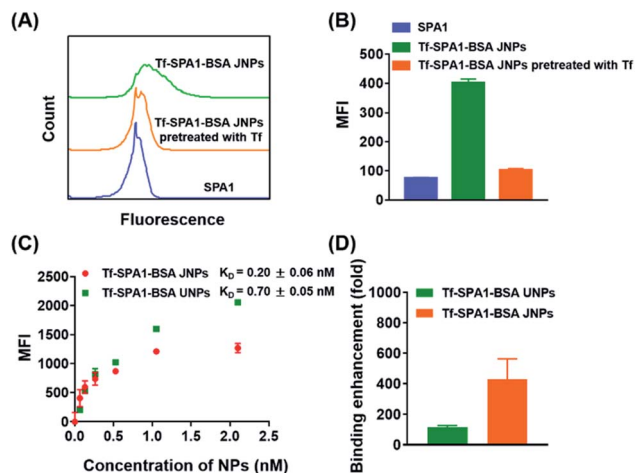


Fig. 2 Targeting of Tf-SPA1-BSA JNPs towards B16F10 tumor cells *in vitro*. Representative flow cytometry histograms (A) and corresponding mean fluorescence intensity (B) of B16F10 cells incubated with FITC-labeled SPA1 and FITC-labeled Tf-SPA1-BSA JNPs in the absence or presence of free Tf. (C) Saturation binding of FITC-labeled Tf-SPA1-BSA JNPs and Tf-SPA1-BSA UNPs to B16F10 cells. (D) Enhancement in the binding affinity of the two nanoparticles in comparison to free Tf. Data are presented as mean \pm SD ($n = 3$).

conjugates.^{28,29} More importantly, the K_D value of Tf-SPA1-BSA JNPs was also lower than that of Tf-SPA1-BSA UNPs, indicating that JNPs have higher binding affinity than uniformly modified nanoparticles. This may lay the foundation for possible enhanced particle-cell interactions.

The above studies demonstrated the construction of a series of JPs with different biofunctionalities. More interestingly, we have discovered that JPs showed a higher binding affinity to tumor cells than UNPs under the same conditions. However, particle-cell interaction studies were conducted with a single cell type. Many important biological processes usually involve different types of cells. For example, in cancer immunotherapy, macrophages or dendritic cells are needed to phagocytose tumor cells for antigen processing. Here, we wonder whether such JPs would be effective in mediating tumor cell-macrophage interaction. Tumor cells overexpress CD47 on membranes, which binds to SIRP α on macrophages to inhibit phagocytosis.³⁰ Blockade of the CD47-SIRP α axis has been shown to increase tumor cell phagocytosis.^{31,32} Thus, in this study, we chosen Tf and aSIRP α to prepare Tf-SPA1-aSIRP α JNPs for the study of particle-mediated interaction between tumor cells and macrophages. On top of this, we would like to validate whether the Tf-SPA1-aSIRP α JNPs could bind to TfRs on tumor cells and SIRP α on macrophages separately. eFluor 670-labeled B16F10 cells or anti-F4/80 labeled bone marrow-derived macrophages (BMDMs) were incubated with Tf-SPA1-aSIRP α JNPs and subjected to flow cytometry analysis (Fig. S5† and 3A, B). As can be seen, both functionalized NPs showed stronger cell binding to either B16F10 tumor cells or BMDMs than each free ligand. Moreover, significantly enhanced cell binding of Tf-SPA1-aSIRP α JNPs in comparison to Tf-SPA1-aSIRP α UNPs was observed in either tumor cells (99.4% vs. 56.7%, $p < 0.001$) or macrophages (99.5% vs. 41.0%, $p < 0.001$),

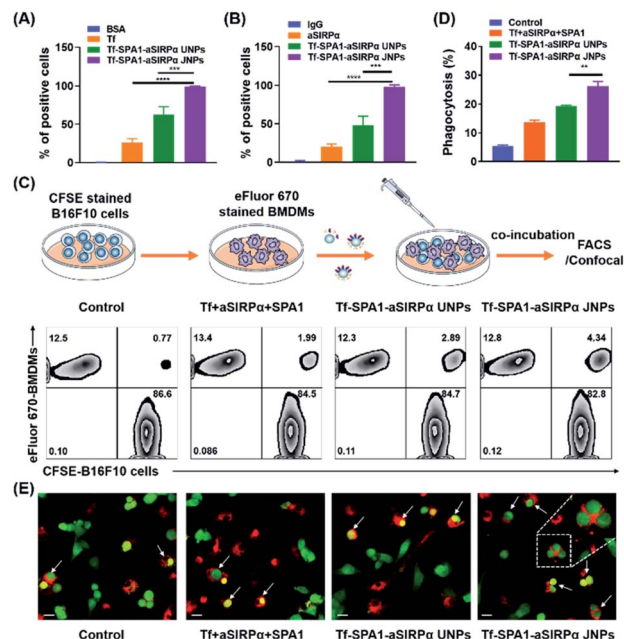
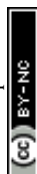


Fig. 3 Tf-SPA1-aSIRP α JNPs facilitate phagocytosis *in vitro*. Relative binding ability of different treatments to B16F10 cells (A) and BMDMs (B). B16F10 cells were labelled with eFluor 670 and BMDMs were labelled with APC anti-F4/80. Data are presented as mean \pm SD ($n = 3$). *** $p < 0.001$; **** $p < 0.0001$. (C) Schematic representation of phagocytosis assay (upper) and representative flow cytometric analysis images of phagocytosis assays treated with different formulations (lower). (D) Relative quantification of phagocytosis of tumor cells by BMDMs. Data are presented as mean \pm SD ($n = 3$). ** $p < 0.01$. (E) Representative confocal images of phagocytosis assays. Scale bar: 20 μ m. In (C), (D) and (E), B16F10 cells were labelled with CFSE (green) and BMDMs were labelled with eFluor 670 (red).

indicating the advantage of Janus structures in mediating cell-particle interactions.

On this basis, we further investigated how the nanoparticles mediated the interaction between the macrophages and tumor cells. eFluor 670-labeled BMDMs and CFSE-labeled B16F10 cells were co-cultured with Tf-SPA1-aSIRP α JNPs and other formulations under the same conditions. Flow cytometry analysis (Fig. 3C and D) indicated that Tf-SPA1-aSIRP α UNPs were able to facilitate phagocytosis of B16F10 cells by BMDMs compared with a physical mixture of free Tf, free aSIRP α , and SPA1 (denoted as Tf + aSIRP α + SPA1) to some extent. The Tf-SPA1-aSIRP α JNPs could mediate an even higher phagocytosis than Tf-SPA1-aSIRP α UNPs (19.4% vs. 25.3%, $p < 0.01$), presumably due to their increased binding affinity to both tumor cells and BMDMs. Moreover, we also employed confocal microscopy to visually observe the nanoparticle-mediated B16F10-BMDM interaction (Fig. 3E), and confirmed that more B16F10 cells could be phagocytosed by BMDMs after co-culture with Tf-SPA1-aSIRP α JNPs.

To observe the phagocytosis of B16F10 cells by BMDMs, 2.30 μ m Tf-SPA3-aSIRP α JNPs were utilized and appeared as blue in pseudo-color, while BMDMs and B16F10 cells showed red and green fluorescence, respectively. As shown in the confocal images (Fig. 4A), we could see that more blue particles bound to



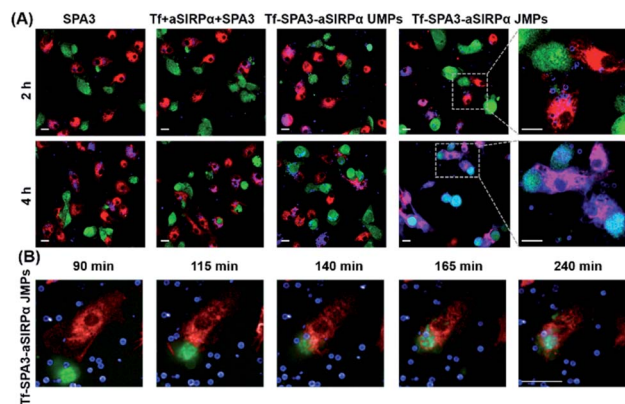


Fig. 4 Tf-SPA3-aSIRP α JMPs promote the interaction and subsequent phagocytosis of B16F10 cells by BMDMs. (A) Representative confocal images of phagocytosis assays treated with different formulations for 2 or 4 h, respectively. (B) Time-dependent of phagocytosis treated with Tf-SPA3-aSIRP α JMPs. In (A) and (B), B16F10 cells were labelled with CFSE (green), BMDMs were labelled with eFluor 670 (red) and particles were labelled with RB (blue). Scale bar: 20 μ m.

BMDMs and B16F10 cells after 2 h co-incubation with Tf-SPA3-aSIRP α JMPs than other groups. With the incubation time extending to 4 h, B16F10 cells became phagocytosed by BMDMs for Tf-SPA3-aSIRP α JMP treatment, which indicates that Tf-SPA3-aSIRP α JMPs might mediate a stronger cell-cell interaction due to their enhanced binding affinity to both cells. To further observe the details, time-course tracking of phagocytosis was performed on a high-content analysis system. In Fig. 4B, we could clearly see the blue Tf-SPA3-aSIRP α JMPs attached to B16F10 cells and BMDMs, with B16F10 cells coming into contact with BMDM gradually and culminating with the phagocytosis of the tumor cells and JMPs together.

Conclusion

In summary, we developed a versatile strategy for the construction of JPs that can be spatially selective for the immobilization of different biomolecules on a single particle. Using Tf as a targeting ligand, we discovered that the dissociation constants of the JPs were significantly lower than those of particles coated uniformly with the same number of ligands, demonstrating that the Janus structure leads to an enhanced binding affinity to tumor cells with Tf-receptor overexpression. More importantly, by manipulating the spatial arrangement of Tf and aSIRP α on the particles, we demonstrated that the biofunctional JPs enable simultaneous targeting of macrophages and tumor cells, and thus facilitate the subsequent phagocytosis of tumor cells. Time-course tracking imaging indicated that the JPs could mediate the phagocytosis process. This study supports the continued development of Janus structures with spatially defined surface functionality for unique biomedical applications.

Conflicts of interest

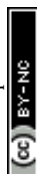
There are no conflicts to declare.

Acknowledgements

This work was supported by the National Key R&D Program of China (2017YFA0205600), National Natural Science Foundation of China (31771091, 51922043, and 81871994), Guangdong Natural Science Funds for Distinguished Young Scholar (2017A030306018 and 2019B151502063), Guangdong Provincial Programs (2017ZT07S054 and 2017GC010304), Outstanding Scholar Program of Guangzhou Regenerative Medicine and Health Guangdong Laboratory (2018GZR110102001), Guangzhou Science and Technology Planning Program (201902020018), and Fundamental Research Funds for Central Universities.

Notes and references

- 1 M. T. Zhu, G. J. Nie, H. Meng, T. Xia, A. Nel and Y. L. Zhao, *Acc. Chem. Res.*, 2013, **46**, 622–631.
- 2 T. J. Merkel, S. W. Jones, K. P. Herlihy, F. R. Kersey, A. R. Shields, M. Napier, J. C. Luft, H. Wu, W. C. Zamboni and A. Z. Wang, *Proc. Natl. Acad. Sci. U. S. A.*, 2011, **108**, 586–591.
- 3 J. Cui, Y. Ju, K. Liang, H. Ejima, S. Lörcher, K. T. Gause, J. J. Richardson and F. Caruso, *Soft Matter*, 2014, **10**, 2656–2663.
- 4 S. Ohta, D. Glancy and W. C. W. Chan, *Science*, 2016, **351**, 841–845.
- 5 L. J. Eggermont, L. E. Paulis, J. Tel and C. G. Figdor, *Trends Biotechnol.*, 2014, **32**, 456–465.
- 6 A. K. Kosmides, K. Necochea, J. W. Hickey and J. P. Schneck, *Nano Lett.*, 2018, **18**, 1916–1924.
- 7 J. W. Hickey, F. P. Vicente, G. P. Howard, H.-Q. Mao and J. P. Schneck, *Nano Lett.*, 2017, **17**, 7045–7054.
- 8 C. S. Chiang, Y. J. Lin, R. Lee, Y. H. Lai, H. W. Cheng, C. H. Hsieh, W. C. Shyu and S. Y. Chen, *Nat. Nanotechnol.*, 2018, **13**, 746–753.
- 9 H. Yuan, W. Jiang, C. A. von Roemeling, Y. Qie, X. Liu, Y. Chen, Y. Wang, R. E. Wharen, K. Yun and G. Bu, *Nat. Nanotechnol.*, 2017, **12**, 763–769.
- 10 M. Xuan, J. Shao, C. Gao, W. Wang, L. Dai and Q. He, *Angew. Chem., Int. Ed.*, 2018, **130**, 12643–12647.
- 11 S. Balasubramanian, D. Kagan, C. M. Jack Hu, S. Campuzano, M. J. Lobo-Castañón, N. Lim, D. Y. Kang, M. Zimmerman, L. Zhang and J. Wang, *Angew. Chem., Int. Ed.*, 2011, **50**, 4161–4164.
- 12 K. Lee, Y. Yi and Y. Yu, *Angew. Chem., Int. Ed.*, 2016, **55**, 7384–7387.
- 13 Y. Yi, L. Sanchez, Y. Gao and Y. Yu, *Analyst*, 2016, **141**, 3526–3539.
- 14 T. Yang, L. Wei, L. Jing, J. Liang, X. Zhang, M. Tang, M. J. Monteiro, Y. Chen, Y. Wang and S. Gu, *Angew. Chem., Int. Ed.*, 2017, **56**, 8459–8463.
- 15 R. Kadam, M. Zilli, M. Maas and K. Rezwan, *Part. Part. Syst. Charact.*, 2018, **35**, 1700332.
- 16 G. Agrawal and R. Agrawal, *ACS Appl. Nano Mater.*, 2019, **2**, 1738–1757.



- 17 M. Zhang, L. Zhang, Y. Chen, L. Li, Z. Su and C. Wang, *Chem. Sci.*, 2017, **8**, 8067–8077.
- 18 Y. Zhang, K. Huang, J. Lin and P. Huang, *Biomater. Sci.*, 2019, **7**, 1262–1275.
- 19 A. K. Salem, P. C. Searson and K. W. Leong, *Nat. Mater.*, 2003, **2**, 668–671.
- 20 Y. J. Son, H. Kim, K. W. Leong and H. S. Yoo, *ACS Nano*, 2013, **7**, 9771–9779.
- 21 Y. Gao and Y. Yu, *J. Am. Chem. Soc.*, 2013, **135**, 19091–19094.
- 22 K. Lee and Y. Yu, *J. Mater. Chem. B*, 2017, **5**, 4410–4415.
- 23 W. He, N. Kapate, C. W. Shields IV and S. Mitragotri, *Adv. Drug Delivery Rev.*, 2019, DOI: 10.1016/j.addr.2019.12.001.
- 24 W. Nie, G. Wu, J. Zhang, L. L. Huang, J. Ding, A. Jiang, Y. Zhang, Y. Liu, J. Li, K. Pu and H. Xie, *Angew. Chem., Int. Ed.*, 2020, **59**, 2018–2022.
- 25 J. Chen, M. Liu, C. Chen, H. Gong and C. Gao, *ACS Appl. Mater. Interfaces*, 2011, **3**, 3215–3223.
- 26 S. Jiang, M. J. Schultz, Q. Chen, J. S. Moore and S. Granick, *Langmuir*, 2008, **24**, 10073–10077.
- 27 J. Y. Yhee, S. J. Lee, S. Lee, S. Song, H. S. Min, S.-W. Kang, S. Son, S. Y. Jeong, I. C. Kwon and S. H. Kim, *Bioconjugate Chem.*, 2013, **24**, 1850–1860.
- 28 C. H. J. Choi, C. A. Alabi, P. Webster and M. E. Davis, *Proc. Natl. Acad. Sci. U. S. A.*, 2010, **107**, 1235–1240.
- 29 W. Jiang, B. Y. Kim, J. T. Rutka and W. C. Chan, *Nat. Nanotechnol.*, 2008, **3**, 145.
- 30 E. J. Lee, G. H. Nam, N. K. Lee, M. Kih, E. Koh, Y. K. Kim, Y. Hong, S. Kim, S. Y. Park and C. Jeong, *Adv. Mater.*, 2018, **30**, 1705581.
- 31 Q. Chen, C. Wang, X. Zhang, G. Chen, Q. Hu, H. Li, J. Wang, D. Wen, Y. Zhang and Y. Lu, *Nat. Nanotechnol.*, 2019, **14**, 89–97.
- 32 F. Zhou, B. Feng, H. Yu, D. Wang, T. Wang, Y. Ma, S. Wang and Y. Li, *Adv. Mater.*, 2019, **31**, 1805888.

